



HAL
open science

Model synthetic pastes for low pH cements

E. Kangni-Foli, Stéphane Poyet, P. Le Bescop, T. Charpentier, F. Bernachy-Barbe, A. Dautères, E. L'Hôpital, M. Neji, J.-B. d'Espinose de Lacaillerie

► **To cite this version:**

E. Kangni-Foli, Stéphane Poyet, P. Le Bescop, T. Charpentier, F. Bernachy-Barbe, et al.. Model synthetic pastes for low pH cements. *Cement and Concrete Research*, 2020, 136, pp.106168. 10.1016/j.cemconres.2020.106168 . cea-02894517

HAL Id: cea-02894517

<https://cea.hal.science/cea-02894517>

Submitted on 25 Jul 2022

HAL is a multi-disciplinary open access archive for the deposit and dissemination of scientific research documents, whether they are published or not. The documents may come from teaching and research institutions in France or abroad, or from public or private research centers.

L'archive ouverte pluridisciplinaire **HAL**, est destinée au dépôt et à la diffusion de documents scientifiques de niveau recherche, publiés ou non, émanant des établissements d'enseignement et de recherche français ou étrangers, des laboratoires publics ou privés.



Distributed under a Creative Commons Attribution - NonCommercial - NoDerivatives 4.0 International License

1 Model synthetic pastes for low pH cements

2 Kangni-Foli E. ^{1,2}, Poyet S. ³, Le Bescop P. ³, Charpentier T. ⁴, Bernachy-Barbé F. ³, Dauzères A. ¹,
3 L'Hôpital E. ¹, Neji M. ¹, d'Espinose de Lacaillerie J.-B. ²

4 (1) IRSN, Institute of Radiation Protection and Nuclear Safety, PSE-ENV/SEDRE/ LETIS, BP 17, F-
5 92262 Fontenay Aux Roses, France

6 (2) Soft Matter Science and Engineering, UMR CNRS 7615, ESPCI Paris, Université PSL, 10 rue
7 Vauquelin, 75005 Paris, France

8 (3) Des-Service d'Etude du Comportement des Radionucléides (SECR), CEA, Université de Paris-
9 Saclay, F-91191, France

10 (4) NIMBE, CEA, CNRS, Université Paris-Saclay, CEA Saclay, F-91191 Gif-sur-Yvette Cedex,
11 France

12

13 **Corresponding author:** Stéphane POYET

- 14 • Postal address: CEA Saclay, DES/ISAS/DPC/SECR/LECBA, B158 PC25, F-91191
15 Gif-sur-Yvette cedex, France.
- 16 • Email: stephane.poyet@cea.fr

17

18 **Conflict of interest:** none

19

20 Abstract

21 Model synthetic pastes were designed to obtain a simplified silica system that could be used in
22 durability studies on materials with low calcium-to-silica ratios. The synthetic pastes made use of
23 the well-known pozzolanic reaction between tricalcium silicate (C_3S) and nanosilica, covering
24 calcium-to-silica ratios (C/S) from 0.8 to 3.0. The pure C_3S paste ($C/S = 3.0$) contained C-S-H and
25 portlandite, while pastes with $C/S < 1.4$ only included C-S-H. The pore solution pH directly
26 correlated with the C/S ratio. The synthetic pastes demonstrated a mineralogy, a C-S-H structure,
27 a mean chain length and pore network features that were similar to ordinary Portland cement
28 (OPC) and low-pH materials, depending on their C/S ratios. The main shortcomings were: (1) high
29 water-to-binder ratio and high superplasticizer dosage to maintain the workability of the
30 synthetic pastes of low C/S ratios and (2) significant cracking of the pastes of low C/S ratios.

31 **Keywords:** Calcium-Silicate-Hydrate (C-S-H) – Model pastes – Microstructure – Mineralogy

32

33 1. Introduction

34 Despite its crucial societal importance, the chemical durability of concrete structures is difficult
35 to predict. This is largely due to the conjunction of a metastable phase assembly in the binder with
36 a multiscale mechanical and porous structure. Correctly predicting crack propagation or reactive
37 transport for example, needs a thorough understanding of the governing phenomena across

38 several length scales [1]: the cement paste at the nano and meso scale [2], the aggregate and the
39 interfacial transition zone at the meso scale [3,4], and finally the structure itself at the macroscale
40 [5]. An unavoidable prelude to multiscale numerical modelling, thermodynamical or mechanical,
41 is thus the understanding of the material at each scale taken separately.

42 Along this line, a lot of progress has been obtained in the last decades by focusing on concrete at
43 the smallest scale: the mineralogical assembly of the cement paste [6–11]. An Ordinary Portland
44 Cement (OPC) paste is in itself a highly complex heterogeneous system made of empty pores,
45 water saturated pores, calcium silicate and aluminate oxides and carbonates. This has led
46 researchers to further simplify the system by restricting the chemistry to the hydration products
47 of tricalcium- (C_3S) or dicalcium- (β - C_2S) silicates [12–19]. It was thus possible to deconvolute the
48 impact of silicates and aluminates chemistry and successfully rationalize non trivial behaviour
49 such as induction and creep [2,19]. However, new needs in term of reduction of CO_2 emission or
50 radioactive waste management has led to the development of low calcium and low pH cement
51 formulation and in particular of the so-called low-alkalinity cements (LAC). Just as for OPC, the
52 long-term prediction of the durability of low-pH cements requires the design of a model chemical
53 system reproducing their main characteristics in terms of mineralogy and porosity.

54 For OPC, the paste formed by hydration of C_3S or β - C_2S constitutes a relevant model of the calcium
55 silicate sub-system since it leads to the precipitation of the two main calcium-bearing hydrates of
56 Portland cements, namely calcium-silicate hydrate (C-S-H) and portlandite (calcium hydroxide,
57 CH). While C-S-H is largely responsible for the mechanical properties of the pastes, portlandite is
58 a key component as it buffers the pH value at 12.5 (at 25°C). This latter fact is not true however
59 for LACs which have very different specificities when compared to OPCs, the main one being the
60 absence of portlandite and a pH of the pore solution (around 11) that is 1 to 3 points lower than
61 in usual cements (≈ 13.5) [20–24]. Such low pH values are commonly achieved by adding
62 significant amounts of secondary cementing materials poor in calcium [25]. As a result, the C/S
63 ratio of the paste is much lower than usual and the development of another chemical model is
64 needed. This is particularly important since the long term durability of LAC is still an open
65 question, especially with respect to carbonation which is highly pH dependent. Consequently, the
66 aim of this paper is to synthesize and describe model synthetic low-pH porous systems
67 representative of LAC pastes.

68 Several attempts have already been presented in the literature. Firstly, Chen *et al.* [26,27] exposed
69 C_3S hardened pastes to ammonium nitrate (6M) in order to dissolve portlandite and lower the
70 CaO/SiO_2 ratio of the C-S-H. Alternatively, other authors created porous compacts of C-S-H
71 powders obtained by aqueous mineral synthesis in excess water [28–37]. Each of these methods
72 demonstrated a main drawback inherent to their fabrication methods, *i.e.* the chemical attack or
73 the mechanical compaction may induce a dissimilarity in the porous medium with regard to that
74 generated by hydration. The chemical attack alters both the hydrates [38] and the pore network
75 [39]. For compacts, comparison with hardened cement pastes does not provide strong evidence
76 of their full representativeness [40]. In addition, compact disintegration subsequent to water
77 immersion has already been observed, which makes them unsuitable for transport modelling [30].

78 More recently, it was shown that pastes made of C-S-H with different C/S ratios could be obtained
79 using a combination of calcium oxide or hydroxide and amorphous silica mixed with water
80 [41,42]. Due to the high water demand of the silica powder [43], the water to solid ratios were
81 high (from 1.1 to 2.0) but could be reduced using a superplasticizer [41]. Chemical analysis of
82 paste obtained in that manner revealed scattered C/S ratios. For instance, in [41], the paste with
83 an average C/S ratio of 1.25 includes areas with C/S ratios of 0.80 and others with C/S of 1.50.
84 This could be the expression of a limited control of the pastes' local chemistry as hydration is
85 known to be controlled by the dissolution rate of C_3S [44–46] which indirectly affects the

86 development of hydrate microstructures [47–49]. The scatter itself is not an issue because it is
 87 representative of real materials [50]. However, within the scope of laboratory studies, more
 88 narrowly distributed C/S ratios could be preferable as they might simplify interpretation of the
 89 results (for example to study the influence of the C/S ratio on the carbonation rate or the
 90 mechanical properties of C-S-H).

91 In this study, we kept the smart idea of Kunther et al. [41] and Maddalena et al. [42] for obtaining
 92 pastes by exploiting the pozzolanic reaction of silica but we investigated another route by
 93 replacing CaO/Ca(OH)₂ by tricalcium silicate. We then synthesized a series of model pastes of
 94 controlled chemistry with narrowly distributed C/S ratios of averages between 0.8 and 3.0. The
 95 methodology used to prepare the model pastes is described and their main chemical,
 96 mineralogical and microstructural properties are detailed. Finally, the relevance of the pastes as
 97 model subsystems for real LAC pastes is discussed.

98

99 2. Materials and methods

100 *Synthesis of the model synthetic pastes*

101 The pastes were prepared using stoichiometric amounts of finely ground C₃S and amorphous
 102 nanosilica (SiO₂) in order to maximise the hydration rate [51–53] and ensure complete silica
 103 reaction [22]. Triclinic C₃S was provided by Mineral Research Processing (Meyzieu, France) and
 104 presented a specific area of 4600 cm²/g. The nanosilica was Rheomac AS 150, provided by BASF
 105 in the form of an aqueous suspension (50 wt%) with a median diameter D50 equal to 100 nm. The
 106 workability of the fresh mix was adjusted using a commercial polycarboxylate superplasticiser
 107 (MasterGlenium Sky 537 from BASF). The pastes were prepared in batches of 1.40 L using a
 108 planetary mixer. Before using expensive C₃S, tests were conducted using OPC with a similar
 109 specific surface to that of C₃S. The tests aimed at determining the most appropriate batching
 110 sequence, water-to-binder ratio (w/b) and superplasticiser dosage. There was no common
 111 workability objective for all the pastes. Our main goal was to obtain pourable pastes: this was easy
 112 without nanosilica but proved to become more and more difficult as the C/S ratio was decreased.
 113 The resulting compositions were then tested using C₃S and modified accordingly. The pastes
 114 incorporated significant amounts of nanosilica (up to 42 wt% for C/S = 0.80, see Table 1); this
 115 induced two major issues: (1) the high water demand of nanosilica [54,55], and (2) the significant
 116 flocculation of nanosilica in the presence of calcium ions [56,57]. Consequently, the w/b ratio and
 117 the SP dosage had to be increased when the C/S decreased. In the case of the paste with a C/S ratio
 118 of 0.80, the w/b ratio and SP dosage reached high values, i.e. 0.78 and 8.0% respectively. Table 1
 119 gives the formulation of the pastes that we were able to produce. The exact batching sequence is
 120 provided in the Supplementary material section.

121

122

Table 1: Composition of the model pastes for 1L

C/S ratio	3.00	1.40	0.95	0.87	0.80
C ₃ S (g)	1218.8	791.7	586.0	563.9	506.2
Colloidal silica slurry (g)	0.0	475.8	664.5	726.3	734.3
Added water (g)	609.4	379.9	264.1	239.3	244.5
w/b ratio	0.50	0.63	0.73	0.72	0.78
Superplasticiser (wt% of binder)	0.0	3.0	8.0	7.0	8.0
Batching time (min)	5	8	15	17	20

123

124 *Reference cement pastes*

125 To assess the representativity of the synthetic pastes, two cement pastes based on CEM I were
126 prepared: an OPC paste (CEM I) and a reference LAC, namely the T₁ blend (mix of CEM I, silica
127 fume and fly ash, see Table 2) proposed by Codina *et al.* [20] and studied later [6,23,58,59]. The
128 reader is referred to the Supplementary materials section for more detail about elemental
129 composition.

130

131

Table 2: Composition of the reference pastes for 1L

Reference materials	T ₁ (CEM I + SF + FA)	CEM I
C/S ratio	0.53	3.3
Cement (g)	470.4	1396.7
Fly ash (g)	378.2	-
Silica fume (g)	406.8	-
Added water (g)	502.2	558.0
w/b ratio	0.40	0.40
Superplasticiser (wt. % of binder)	1.0	0.0
Batching time (min)	5	5

132

133 The SP dosage of the model synthetic pastes - especially for the lower C/S ratios (0.95, 0.87 and
134 0.80) - was quite high compared to the reference cement pastes. It should be pointed out that
135 nanosilica was incorporated in the model paste, whereas silica fume and fly ash were used in the
136 reference paste. This is why the SP dosage had to be increased to partially offset the water demand
137 of the fine nanosilica particles.

138

139 *Mineralogical and chemical characterisation*

140 The pH of the pore solution was measured using the *ex situ* leaching (ESL) method [60–62]. Owing
141 to the absence of alkalis in the binders, ESL is known to yield similar results with respect to the
142 reference method (extraction).

143 Thermogravimetric analysis (TGA) was performed using a Netzsch STA 409 PC Luxx apparatus.
144 Analyses were run under a constant N₂ flowrate (80 ml/min). The weight losses were recorded
145 from 25°C to 1150°C with a heating rate of 10°C/min [63]. The quantification of portlandite (using
146 the tangential method [64]), expressed in mol/L of paste is obtained by considering the weight
147 loss (between 420–580°C) associated to 120 mg of powdered sample of each model paste and their
148 saturated volumes and apparent densities.

149 Powder X-ray diffraction (XRD) patterns were collected using a XPD PANalytical X'Pert
150 diffractometer with a Bragg-Brentano geometry in an θ - θ configuration and a Cu K α radiation
151 source (45 kV, 40 mA).

152 Silicon magic-angle spinning nuclear magnetic resonance (²⁹Si MAS NMR) single-pulse data was
153 collected using a Bruker Avance III 500 spectrometer operating at the Larmor frequency
154 resonance of 99.3 MHz. Conditions were set to $\pi/2$ pulses of 3.5 μ s, recycle delays of 20 s, spinning
155 in 7 mm zirconia rotor at 5.5 kHz, and a minimum of 4000 scans for each spectrum.
156 Tetramethylsilane was used as an external standard (0 ppm) to report the chemical shifts. The
157 ²⁹Si MAS NMR results were processed using an internally developed software [65,66]. The spectra

158 were fitted using gaussian-lorentzian lineshapes with chemical shifts and widths kept identical
159 for all pastes (see Table 4 and Table S 1).

160 A ZEISS EVO MA15 scanning electron microscope (SEM) equipped with a Quantax detector for
161 energy-dispersive spectrometry (EDS) was used for chemical mapping together with
162 backscattered electrons (BSE) imaging. Acquisitions were collected at 15 kV and 1 nA. Pastes were
163 freeze-dried, mounted using epoxy resin, and then polished using an alcohol-based diamond
164 suspension. Grids of 609 points recorded at 200× magnification were acquired for each sample.
165 Due to the working voltage used, an electron-matter interaction depth of about 1-10 µm within
166 the material was generated.

167

168 *Microstructure characterisation*

169 Microtomographic projections were acquired on a Bruker SkyScan1173 device equipped with a
170 flat detector (2240 × 2240 pixel) using the following operating conditions: 115-130 kV and 61-
171 69 µA. We obtained 360° scans with a rotational step of 0.3°, exposure time of 1100 ms, a frame
172 averaging from 8 to 10, and images with a pixel size of 16.8 µm.

173 The porosity and density of the pastes were obtained using the buoyancy method. Firstly,
174 cylinders were re-saturated under vacuum and water [67], and their volume and weight were
175 measured. They were then dried at 80°C in the presence of CaCl₂ and 105°C until constant weight
176 was reached in order to compute porosity. The rationale behind the choice of these temperatures
177 is that at 80°C, the hydrates are fully preserved but some water remains in the porosity, while at
178 105°C, all water is removed but the hydrates are partially dehydroxylated.

179 The pore entry size distribution (PSD) of the pastes was characterised using mercury intrusion
180 porosimetry (MIP) with a Micromeritics Autopore IV. Prior to the tests, the specimens were
181 crushed into centimetric pieces that were immersed in liquid nitrogen and then freeze-dried for
182 24 hours.

183 The C-S-H content of the pastes was estimated using the method proposed by Olson and Jennings
184 [68] based on the quantification of the water content at 20% RH. Here we did not strictly follow
185 the protocol recommended by Olson and Jennings. Rather we estimated the water content at 20%
186 RH using a desorption experiment and a sorption balance (DVS Advantage). Acquisitions were run
187 at 25°C ±0.1°C, and the automatic 'dm/dt' mode was set for the relative humidity (RH) decrease.
188 Prior to analysis the pastes were crushed and sieved in a CO₂-free glove box. Particles exceeding
189 150 µm were eliminated by sieving and the powders saturated using deionized water. More
190 details can be found in [69]. Such an approach offered a very significant gain of time but might
191 have overestimated the C-S-H content due to the hysteresis between the adsorption and
192 desorption path. The reader should also be aware that the method of Olson and Jennings assumes
193 that the C/S ratio of the C-S-H is equal to 1.7. It is thus well suited for the C₃S and CEM I pastes but
194 subject to caution for other formulations. This might have induced additional uncertainties in the
195 C-S-H quantification process. This point would require more attention but is not addressed in the
196 present work.

197

198 **3. Results**

199 *Reference cement pastes*

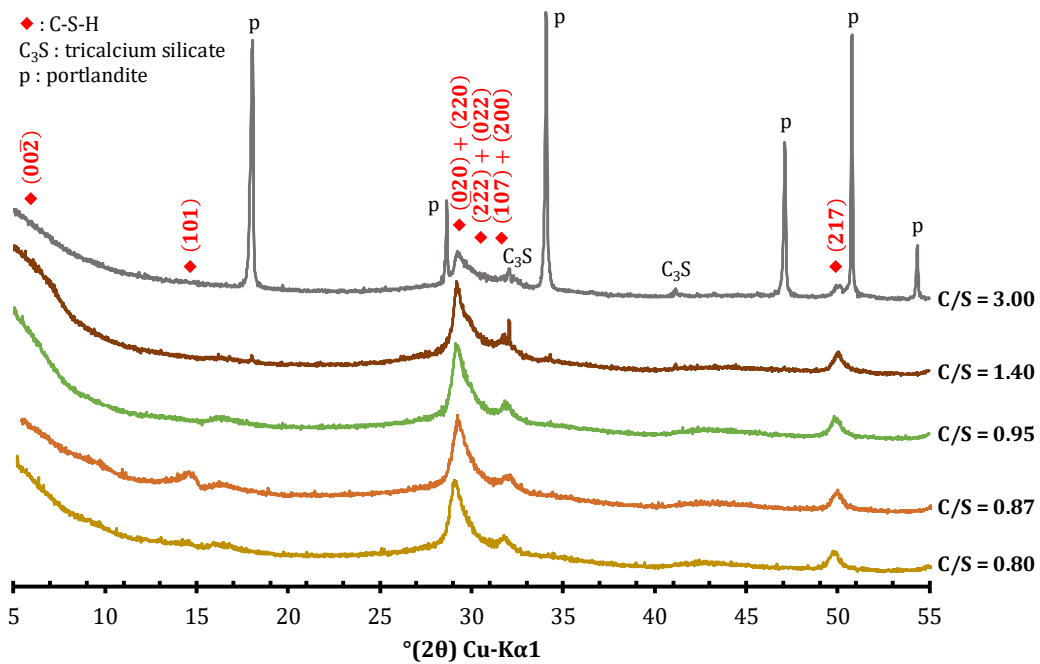
200 The characteristics of reference cement pastes, OPC or LAC were fully in line with what was
 201 expected from the literature and need not to be extensively reported here (see later the NMR
 202 spectra in Figure 3, the MIP in Figure 8 and XRD in Figure S 2). The main difference in terms of
 203 mineralogy for the LAC compared to OPC is the absence of portlandite and the presence of
 204 calcium-bearing amorphous silica (silica gel) and remnants of amorphous silica phase such as fly
 205 ash and silica fume that have not reacted with calcium. Furthermore, the low C/S ratio resulted in
 206 longer dreierketten chains in the C-S-H of the LAC cement paste. The porosity of the LAC paste
 207 presented a more refined pore structures due to pore filling by precipitation of pozzolanic C-S-H.

208

209 *Mineralogy of the model synthetic pastes*

210 X-ray diffractograms of the model pastes with C/S ratios from 0.80 to 3.00 are shown in Figure 1.
 211 The paste with a C/S ratio of 3.00 corresponds to the sample prepared without silica. Logically, its
 212 diffractogram corresponded to what was expected from the hydration of pure C₃S, *i.e.* it mainly
 213 showed diffraction peaks of the portlandite and C-S-H patterns [70–73]. Only traces of reflections
 214 corresponding to remaining C₃S were detected, indicating that hydration was almost complete
 215 [18]. Pastes with C/S ratios of 1.40 mainly displayed C-S-H signals and traces of portlandite and
 216 unreacted C₃S. Finally, for C/S ratios lower than 1.40, the diffractograms only exhibited the C-S-H
 217 diffraction pattern.

218



219

220 *Figure 1: XRD patterns of the synthetic pastes. As the C/S ratio decreases, Portlandite reflections progressively*
 221 *disappeared from the diffractogram. While still barely visible at C/S 1.4, they were absent for synthetic pastes of lower*
 222 *C/S ratios. C-S-H indexing was based on [74–76], ICDD files CH: 44-1481, C₃S: 31-0301.*

223

224 TGA confirmed the results obtained using XRD. The portlandite content measured in the C₃S
 225 paste (7.3 mol/L of paste, cf. Table 3) was very close to that of a fully hydrated C₃S paste
 226 (7.0 mol/L of paste with C-S-H with C/S = 1.70). For C/S ratios of 1.40, losses associated with
 227 C-S-H and traces of portlandite were observed (Figure 2). For C/S ratios lower than 1.40, the

228 thermograms only exhibited signals related to C-S-H (see the C/S = 0.80 thermogram in Figure
 229 2).

230

231 *Table 3: Composition and properties of the synthetic and reference pastes obtained by TGA, μ CT and the buoyancy*
 232 *method. The C-S-H content was obtained following the method of Olson and Jennings [53]. (see Materials and method*
 233 *section)*

C/S ratio	Model pastes					Reference pastes	
	3.00	1.40	0.95	0.87	0.80	CEM I	T ₁
C/S of the C-S-H	1.70	1.40	0.95-1.10	0.87-1.00	0.80-1.00	1.70	[0.8-1.1]*
Porosity (80°C)	38%	52%	57%	57%	58%	36%#°	41%#°
Porosity (105°C)	41%	56%	61%	61%	62%	38%#°	43%#-46%*°
Saturated density	1.89	1.76	1.68	1.67	1.63	2.04*°-2.05#	1.73*°-1.77#
C-S-H (mol/L of paste)	5.6	7.0	6.7	7.0	6.3	5.1*°-5.2°	7.4*°-7.6°
CH (mol/L of paste)	7.3	0.0	0.0	0.0	0.0	5.6*°-5.3#	0.0*#
Cracking (μ CT)	-	-	+	++	++	-	-
	- no crack observed	+ few small cracks			++ several extended cracks		
	data from *[77], °[23], *[20], #[78] *°[79]						

234

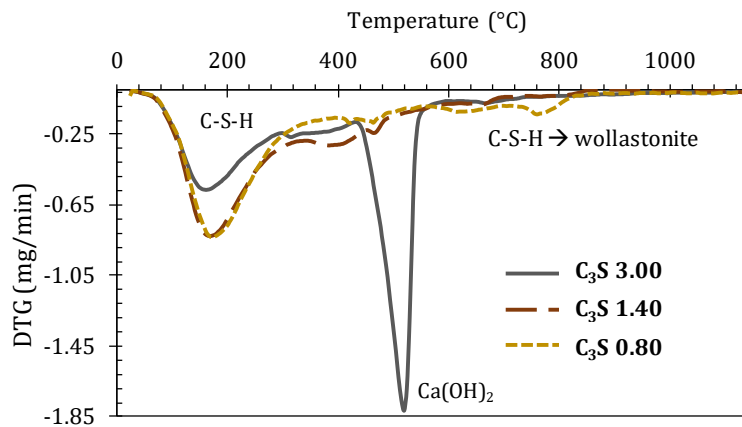


Figure 2: DTG of the model pastes. Besides losses due the removal of water within C-S-H, the typical thermal loss of portlandite was massively observed in the C₃S paste. In contrast, only a residual portlandite content was evidenced in the C/S = 1.40 paste, and it totally disappeared at lower C/S ratios.

235

236 The ²⁹Si MAS-NMR spectra of the pastes are shown in Figure 3. The spectra of the higher C/S ratios
 237 (3.00 and 1.40) samples exhibited the usual resonances attributed to silica tetrahedra sharing one
 238 (Q¹) or two (Q²) oxygen atoms with another tetrahedra at -79.19 ppm and between -83 and -86
 239 ppm respectively [41,80,81]. As expected, the decrease in the C/S ratio resulted in a relative
 240 increase in the Q² contribution reflecting the increase of the length of the dreierketten chains of
 241 the C-S-H. The spectra of pastes with C/S ratios lower than 1.40 predominantly showed Q² silicate
 242 tetrahedra. In that case, the bridging and the paired tetrahedra of the dreierketten chains of C-S-H
 243 (Q^{2b}, Q^{2p}) could also be distinguished. According to the literature, they occur around -83.0 ppm
 244 and -85.0 ppm [82,83]. A broad contribution in the frequency range of Q³ tetrahedra (-90 to -100
 245 ppm) was detected in samples with C/S below 0.95 in increasing amounts as the C/S ratio
 246 decreased (and the silica content of the formulation increased). Q³ coordination has been
 247 proposed in C-S-H of low C/S ratios but are expected to be a minor occurrence in the absence of
 248 aluminium [84]. Without further evidence, and considering its breadth, it was thus preferred to
 249 attribute tentatively this resonance to the occurrence of an amorphous silica (Q³gel). The

250 distribution of the silicate tetrahedra environment as a function of the C/S ratio was obtained by
 251 decomposition of the ^{29}Si resonances and reported in Table 4. Examples of the decomposition
 252 procedure and results are provided as Supplementary materials.

253

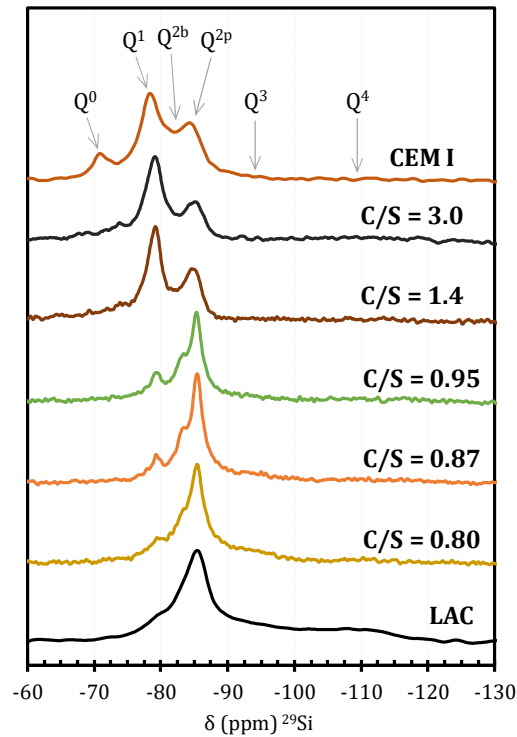


Figure 3: ^{29}Si MAS-NMR spectra of the series of model synthetic pastes with varying C/S ratios and of the reference pastes. Synthetic pastes of higher C/S ratio had lower proportion of Q^2 (middle chain) to Q^1 (end chain) silicate coordination evidencing the expected decrease in dreierketten chain length with increasing C/S ratios. The spectra of the end members of the synthetic series were very similar to the ones of the reference pastes. The reference CEM I and LAC pastes showed Q^0 on the one hand, and Q^3 and Q^4 resonances on the other hand, due to unreacted calcium silicates and to unreacted silica fume and fly ash respectively.

254

255 Table 4: Relative occurrence of silicate environments in the reference and model pastes from ^{29}Si MAS-NMR. For the LAC
 256 paste, unreacted fly ash was observed in the LAC paste characterized by Q^3 and Q^4 broad peaks overlapping with almost
 257 all other resonances.

Paste	Q^0	Q^1	Q^{2b}	Q^{2p}	Q^3 (*)	Q^3 (FA)	Q^4 (FA)	Q^4 (SF)
δ (ppm)	-71.6	-79.2	-83.1	-85.4	-92.0	-90	-104	-110.0
Model pastes								
0.80	-	10%	21%	43%	26%	-	-	-
0.87	-	14%	25%	50%	11%	-	-	-
0.95	-	16%	25%	51%	8%	-	-	-
1.40	-	52%	13%	29%	6%	-	-	-
3.00	-	68%	11%	21%	-	-	-	-
Reference pastes								
CEM I	11%	56%	11%	22%	-	-	-	-
LAC	-	8%	17%	34%	6%	15%	15%	5%

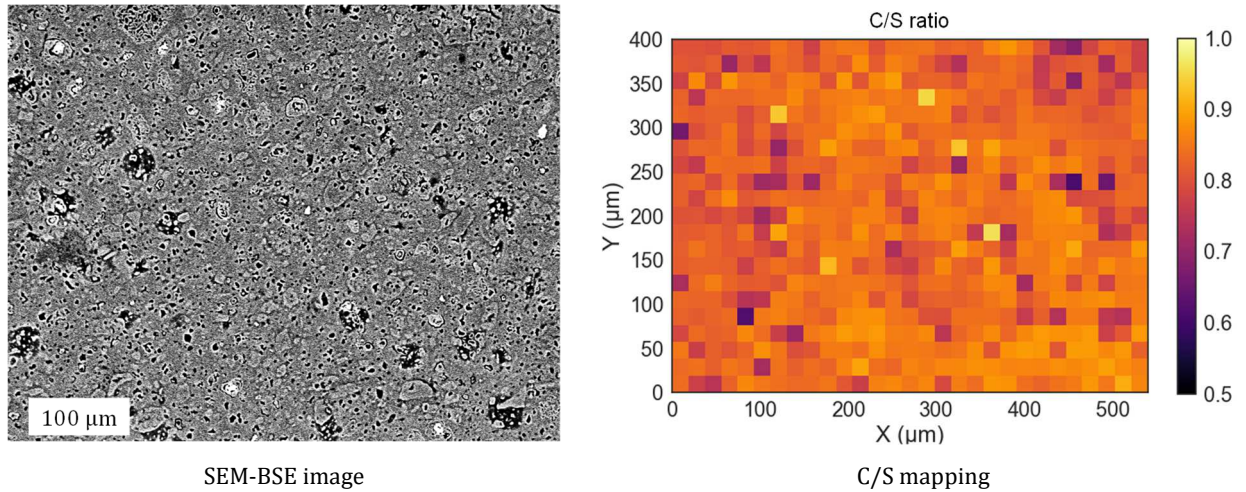
* in the presence of Q^3gel it was not possible to determine the contribution of the Q^3 environments: the Q^3 column then includes the contributions of Q^3 and Q^3gel (when present, i.e. for $\text{C/S} \leq 0.95$)

258

259 Figure 4 shows the chemical analysis (SEM) results obtained for the model synthetic paste with
 260 the lowest (0.80) C/S ratio. A typical electron density contrast image given by BSE mapping is
 261 shown in Figure 4(a) and the subsequent mapping of the C/S ratio distribution obtained using

262 EDS on a $400 \times 550 \mu\text{m}^2$ (21×29 points) subzone is displayed in Figure 4 (b). These results revealed
 263 an almost homogeneous distribution of the C/S ratio at the scale of EDS sampling ($20 \times 20 \mu\text{m}^2$
 264 surface with an analysis depth of $\sim 1\text{-}10 \mu\text{m}$) with a limited standard deviation (coefficient of
 265 variation $\text{CV} = 5\%$).

266



267 *Figure 4: SEM examination of the synthetic paste with a C/S ratio of 0.80. At the scale of the EDS mapping, the paste*
 268 *appeared very homogeneous in composition.*

269

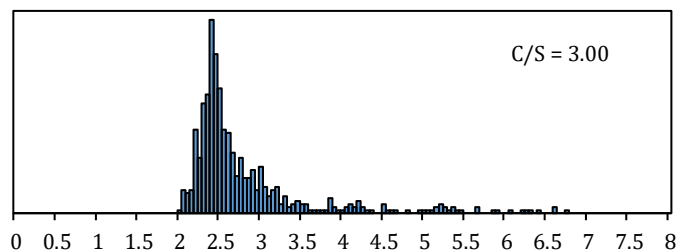
270 Figure 5 and Figure 6 show the C/S ratio occurrence in each model synthetic pastes. All the
 271 samples presented average C/S ratios that were very close to targets except the C_3S paste results
 272 that were scattered over a wider range probably due to the expected precipitation of portlandite
 273 crystals. In contrast, the other samples were narrowly distributed with a CV between 5% and 6%,
 274 with the exception of the paste with a C/S ratio of 0.95 with a CV of 12% (Table 5).

275
 276

Table 5: Mean value and standard deviation of the C/S ratio distribution of the model pastes

Target C/S	0.80	0.87	0.95	1.40	3.00
Average C/S value	0.83	0.89	1.06	1.36	2.53
Standard deviation	0.04	0.05	0.10	0.08	0.31
Coefficient of variation (CV)	5%	6%	9%	6%	12%

277



278

279

Figure 5: Distribution of the CaO/SiO_2 ratio obtained using SEM-EDS for the C_3S paste

280

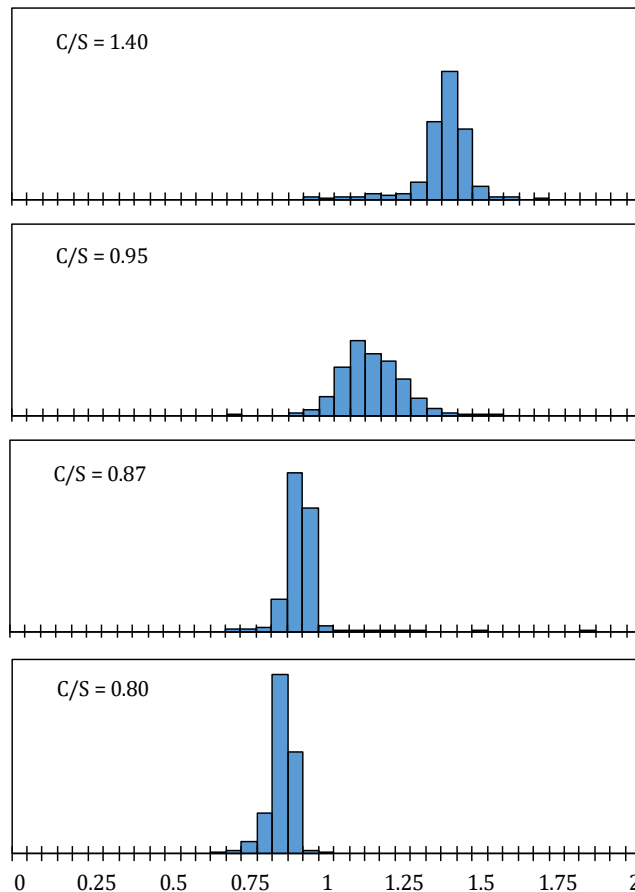


Figure 6: Distribution of the CaO/SiO₂ ratios obtained using SEM-EDS for the synthetic pastes for C/S ≤ 1.40

281

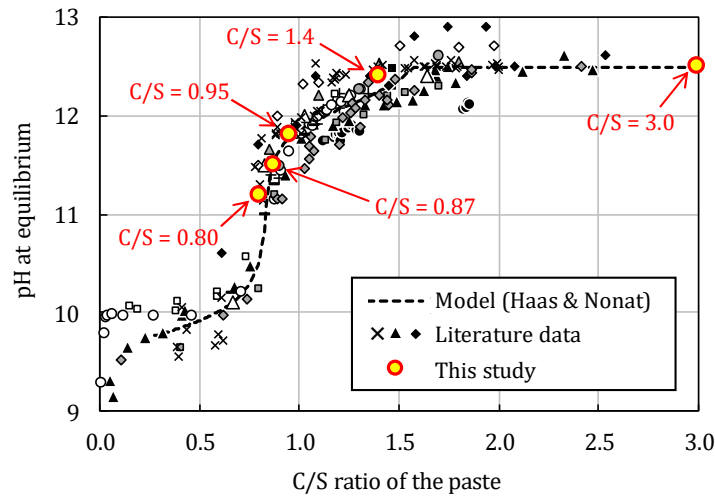
282

283 *Representativity of the chemistry and mineralogy of the model synthetic pastes*

284 XRD and TGA proved that the pastes with C/S ratios lower than 1.40 contained C-S-H only,
 285 whereas the paste based on pure C₃S showed the concomitant precipitation of portlandite. This is
 286 in line with what is expected from a LAC and a CEM I paste respectively. ²⁹Si MAS-NMR analysis of
 287 the pastes evidenced C-S-H silicates silicon environment distribution evolving continuously with
 288 the C/S ratio between what is observed in a LAC and in a CEM I paste. Furthermore, EDS chemical
 289 analysis highlighted the relative homogeneity of the C-S-H pastes with actually an even narrower
 290 scatter in the C/S ratios, compared to those usually observed in cementitious materials but in line
 291 with what is observed in pure calcium silicate hydrate pastes [85,86]. In that respect, the synthetic
 292 pastes formed a representative model of the silicates mineralogical assembly found in LAC pastes.

293 The pH values of the pore solutions obtained using the ESL method are given in Figure 7. For the
 294 purpose of comparison, the values are plotted together with literature data and with the model
 295 proposed by Haas & Nonat [87]. The pH of the synthetic pastes pore solution (measurement made
 296 at 20 ± 2°C, with temperature compensation) demonstrated a decrease while the target C/S ratios
 297 were lowered. Our data falls within the variance shown by literature data and confirmed that the
 298 model synthetic pastes also successfully reproduced the low-pH character of LAC pastes.

299



300

301 *Figure 7: pH of the pore solutions of the synthetic pastes measured using the ex-situ leaching method, redrawn from*
 302 *[12,88–98] along with the model proposed by Haas & Nonat [87]. The pH of the pore water of the synthetic pastes*
 303 *satisfactorily reproduced observations reported in the literature and conformed to the predictive model.*

304

305 *Microstructure of the model synthetic pastes*

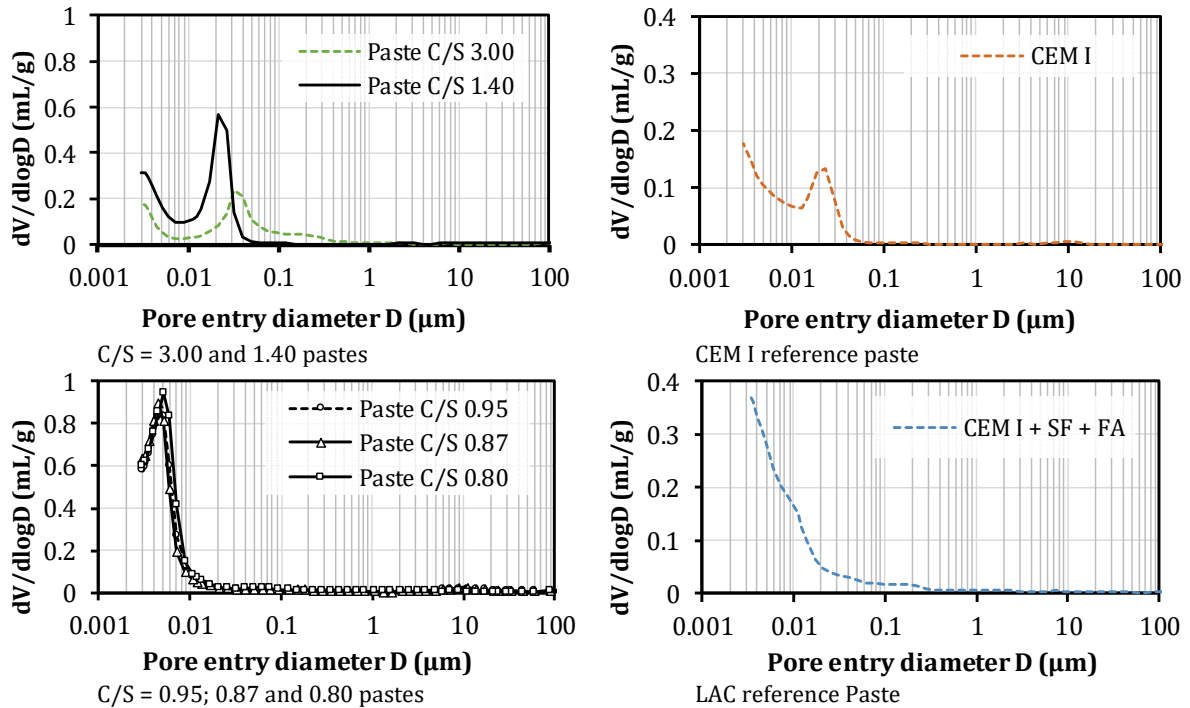
306 The saturated density, porosity and chemical composition (C-S-H and CH contents) are reported
 307 in Table 3. The estimated C-S-H content was higher for the pastes with C/S ratios lower than 3.00:
 308 this was in line with the expected formation of extra C-S-H from silica through pozzolanic
 309 reactions. The paste porosity increased and the density decreased when the target C/S ratio
 310 decreased. However, as the C/S ratio was decreased by addition of nanosilica, a concomitant
 311 increase of the w/b ratio was needed to maintain the workability of the synthetic pastes. The
 312 variations in porosity and density was thus probably more associated to the water content than
 313 to a change of chemistry. Figure 8 illustrates the pore size distribution (PSD) of the synthetic
 314 pastes obtained by MIP. For sake of comparison, the cement pastes are also presented. While the
 315 PSD of the pastes with C/S ratios of 3.00 and 1.40 revealed the expected presence of the C-S-H gel
 316 porosity in the 10 nm range, the pore structure was considerably refined for the lower C/S ratio.
 317 Again, this could be related to the filling effect induced by the precipitation of pozzolanic C-S-H.
 318 The increase of the porous volume on the other hand was probably related to the increased w/b
 319 ratios of the synthetic pastes.

320

321 *Representativeness of the microstructure of the model synthetic pastes*

322 The synthetic pastes had a narrower PSD and a higher pore volume than the one of the reference
 323 LAC paste, again due to the w/b ratio needed for their mixing as previously stated in the Materials
 324 and methods section. However, the PSD of the low C/S synthetic pastes had no pores with critical
 325 entry diameter above 10 nm (Figure 8). This was reminiscent of what is observed in LAC pastes
 326 where the paste capillary porosity is considerably reduced by the pozzolanic reaction.

327



328 *Figure 8: PSD from mercury intrusion porosimetry for reference (right) and synthetic pastes (left). The PSD of the high*
 329 *C/S ratio synthetic pastes conformed to the one of an OPC (CEM I) paste, and the one for the lower C/S ratios to the one of*
 330 *the LAC (CEMI+SF+FA) reference paste.*

331

332 X- μ CT scans of samples with C/S ratios of 1.40, 0.87 and 0.80 are shown in Figure 9. The C/S ratio
 333 of 1.40 showed a homogenous matrix, almost exempt of air bubbles. No cracks were observed in
 334 the pastes with the higher C/S ratios (3.00 and 1.40) (image a). The pastes with lower C/S ratios
 335 of 0.87 and 0.80 exhibited more contrasted features with darker spots observed in the matrix;
 336 these areas could be attributed to silica-enriched areas, thus supporting the NMR observation of
 337 a small amount of unreacted silica. These pastes also contained several bubbles due to reduced
 338 workability induced by the high amount of nanosilica in their formulations. Furthermore, they had
 339 an extended crack network (images b, c). The cracks made the samples very brittle and it was
 340 necessary to be extremely careful when handling the low C/S synthetic pastes and they proved to
 341 be very difficult (almost impossible) to cut without breaking. This was believed to be due to the
 342 polymerisation of the silica chains of the C-S-H induced by the incorporation of silica in the C-S-H,
 343 which is known to generate significant volume changes [27] and might result in densification and
 344 internal stress during maturation of the lower C/S pastes. It must be mentioned though that the
 345 unusually high superplasticizer dosage might have played a role in the brittleness of the pastes of
 346 low C/S ratios even though the literature remains scant about this subject. Ramachandran [99]
 347 showed that lignosulfonates had strong and irreversible interactions with the C-S-H but it was
 348 later proven that more recent compounds [100] such as melamine sulfonates and polyethylene
 349 oxide phosphonates did not affect the C-S-H [101,102]. The results are however not so clear with
 350 polycarboxylic ethers [103–106]. This point would require more attention in the future.

351

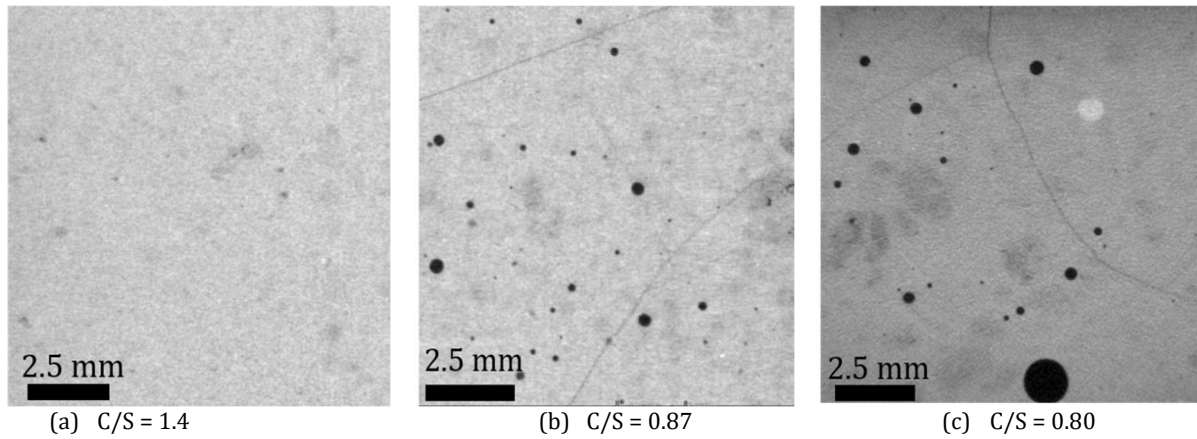


Figure 9: X-ray μ CT scans images of 3 samples of the synthetic pastes series. Significant cracking was observed in paste with lower C/S ratios

352
353

354

355 4. Discussion

356 At first sight and as exposed in the results section, the mineralogical assembly of the model
357 synthetic pastes seemed to correctly represent the one expected from LAC pastes. To examine
358 further this issue, the atomic and molecular structure of their C-S-H, as revealed by NMR, was
359 examined in details and compared to the ones of cement pastes.

360 It is common practice to estimate the mean chain length (MCL) of the C-S-H dreierketten silicate
361 chains from the distribution of the silicate environment obtained by ^{29}Si MAS-NMR. Accordingly,
362 the MCL was obtained in the synthetic pastes using the C-S-H crystal chemical model of
363 Richardson [107]. Indeed, the following simplified expression (Equation 1) relates the MCL to the
364 NMR relative intensities of the Q^1 and Q^2 (Q^{2b} and Q^{2p}) environments:

$$\text{MCL} = 2 \left(\frac{Q^1 + Q^{2b} + Q^{2p}}{Q^1} \right) \quad \text{Equation 1}$$

365

366 Figure 10 shows the C-S-H MCL of the pastes depending on their targeted C/S, along with
367 predictions from the Richardson tobermoritic model and some data from literature. In the higher
368 C/S range (above 1.5), the C-S-H of the pastes demonstrated a chain length variation that was not
369 fully described by the simple tobermoritic model. This behaviour is similar to what is commonly
370 observed in cement paste and is rationalized through an additional charge compensation
371 mechanism, which involved calcium insertion in interlayers [107,108]. However, within the lower
372 C/S domain ($C/S \leq 1.0$), the mean chain length of the C-S-H in the synthetic pastes followed
373 reasonably well the prediction of a tobermoritic behaviour.

374

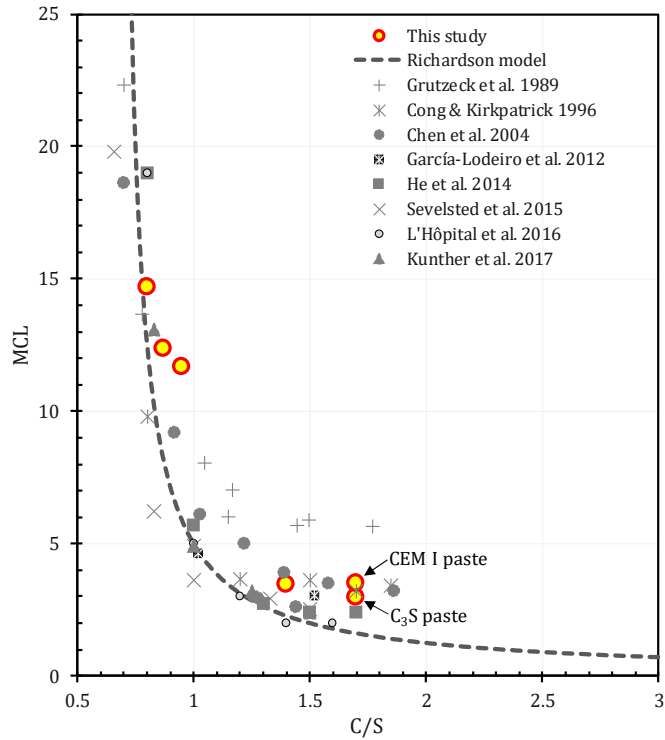


Figure 10: C-S-H mean chain length of the synthetic pastes (from ^{29}Si MAS NMR) along with literature data [12,41,83,89,90,107,109–111]. The MCL obtained for our model pastes correlated well with the MCL of the cementitious materials reported in the literature

375

376
377
378

379

380 In the crystal-chemical structure provided by Richardson [107], the C-S-H gel is considered as a
381 structurally defective form of tobermorite. The structural model describes the C-S-H structure
382 (MCL, C/S ratio) based on the rate of occupancy of the vacant sites. Adopting this structural model,
383 one can in principle back-calculate the C/S ratio of the C-S-H from the NMR spectrum. Practically
384 speaking, following Richardson [107], the C/S ratio (Equation 2) and the mean chain length (MCL)
385 were calculated using:

$$\text{MCL} = \frac{1 - \nu}{\nu} \quad \text{and} \quad \frac{C}{S} = \frac{\frac{2}{3} + \nu}{1 - \nu} \quad \text{Equation 2}$$

386 where the fraction of vacant sites ν (Equation 3) within the C-S-H structure was evaluated by
387 decomposition of the NMR contributions:

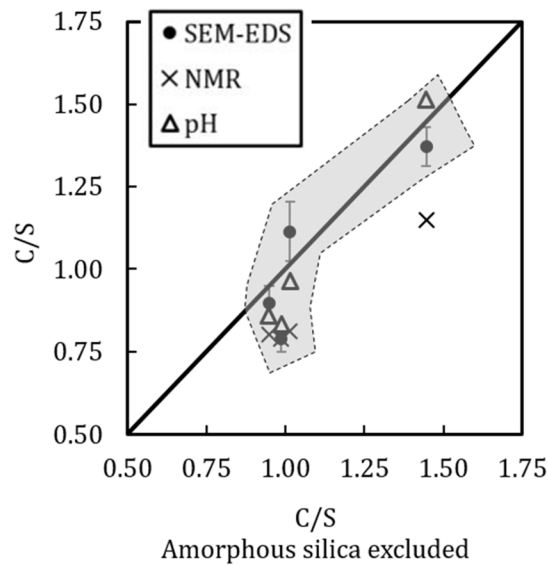
$$\nu = \frac{\frac{1}{2}Q^1}{\frac{3}{2}Q^1 + Q^2 + Q^3} \quad \text{Equation 3}$$

388 Excluding the Q^3 resonance attributed to a silica gel, the C/S ratio predicted from the Richardson
389 defective tobermoritic model agreed reasonably well with the bulk C/S ratio of the pastes (Figure
390 11). This meant not only that the pastes were indeed devoid of portlandite, as seen by XRD and
391 TGA, but also that their C-S-Hs' structure behaved identically to the ones encountered in real (LAC)
392 cement paste where the defective tobermorite structural model is now well established [112].
393 This confirmed the representativeness of the mineralogy of synthetic pastes' silicate with respect
394 to the one of LAC paste of identical C/S.

395 Finally, it might be useful to stress the fundamental difference between the C/S pertaining to NMR
396 on the one hand and to SEM-EDS analyses and to the pH of the pore solutions on the other hand

397 (Figure 11). NMR analyses account for properties at the molecular scale and thus reflects the local
398 availability of Ca and Si at the C-S-H scale. In contrast pH is a macroscopic property reflecting
399 phase equilibria within the sample, namely C-S-H and portlandite. Lastly, SEM-EDS probes the
400 sample at the micro scale and its mean value is thus expected to reproduce the bulk composition
401 of the paste within experimental errors. These considerations are illustrated in Figure 11 where
402 C/S ratios obtained by SEM-EDS and by modelling the ^{29}Si NMR spectra as well as the pH are
403 compared to the bulk C/S ratio recalculated excluding the silicon incorporated in amorphous silica
404 (estimated from the ^{29}Si NMR spectra). The latter C/S ratio was taken as being the one of the
405 C-S-H / portlandite assemblage.

406



407

408 *Figure 11: Comparison of the bulk C/S ratios (excluding the silicon in the amorphous non C-S-H part of the sample,*
409 *unreacted products or silica gels, estimated by ^{29}Si NMR) with the results of SEM-EDS and with the ones expected from*
410 *modelling pH measurements (Haas and Nonat model) and NMR ones (Richardson model). Error bars on the SEM-EDS*
411 *data correspond to the measured coefficient of variation (see Table 5). The accuracy of the pH measurements are +/-*
412 *0.05. This translates into an error of about +/- 0.01 in the C/S values given by the Haas and Nonat model (Figure 7). The*
413 *NMR intensities are obtained with an accuracy of about 10% leading to an error of about +/- 0.05 in the C/S values given*
414 *by the Richardson model (Figure 10).*

415

416 5. Conclusions and perspectives

417 In this study we prepared a series of synthetic pastes with C/S ratios between 0.8 and 3.0 and
418 evaluated its potential as a model silicate subsystem for LAC pastes. From a chemical and
419 mineralogical standpoint, the synthetic pastes appeared as good models, reproducing
420 satisfactorily the mineralogical assemblage. The structure of the C-S-H and the amount of
421 portlandite formed, or not, followed what was expected from a LAC paste. Furthermore, the pH of
422 the pore solutions also conformed very well to predictions with respect to the C/S ratios. This
423 objective was met by choosing C_3S and nanosilica with the appropriate dosage. However, the use
424 of nanosilica induced a high water demand and the formulation had to be optimized through an
425 increased w/b ratio and high superplasticiser dosage. Consequently, the synthetic pastes had a
426 higher pore volume. All the while, the evolution of the PSDs of the synthetic pastes with the C/S
427 ratio was similar to those of the reference pastes. The protocol proposed in the present work thus
428 constituted an interesting route to design synthetic pastes to model the silica subsystem of LAC

429 pastes. This might be particularly useful to model experimentally complex reactive transport
430 within low-pH cements, such as carbonation. In addition, since a narrow variation of C/S ratios
431 was obtained for each targeted value, this series could be suitable for studying the influence of the
432 C/S ratio on various properties of cementitious materials, such as the C-S-H gel mechanical
433 properties. Such studies will have to factor in however, the fact that the pore volume of the model
434 pastes were much higher than those usually encountered in real cement pastes.

435 The present work intended to study specifically the role of the C/S ratio of the silicate phases but
436 it is understood that real pastes, and in particular LAC formulations [22, 29], include significant
437 amounts of aluminium. The influence of aluminium on low-pH pastes will thus have to be
438 investigated.

439 Finally, to be complete, it must be emphasised that one of the main shortcomings of these model
440 synthetic pastes was their tendency to crack; the density of cracks increased when the C/S ratio
441 decreased. This was assumed to be an intrinsic property due to the polymerisation of the C-S-H
442 induced by incorporation of silicate in the C-S-H during the pozzolanic reaction. Indeed, chain
443 length variation is known to generate change in volume [27]. Yet the reader should keep in mind
444 that the unusually high superplasticizer dosage might have also played a significant role in the
445 brittleness of the model pastes. Shaping test samples for transport studies will thus require
446 particular care.

447

448 **Acknowledgments**

449 The financial support for this work was provided by IRSN and CEA. Helpful discussions with
450 Prof. B. Lothenbach (EMPA, Switzerland) and Prof. J. Skibsted (Aarhus University) are gratefully
451 acknowledged.

452

453 **References**

- 454 [1] N. Seigneur, É. Kangni-Foli, V. Lagneau, A. Dauzères, S. Poyet, P. Le Bescop, E. L'Hôpital, J.B.
455 d'Espinose de Lacaillerie, Understanding the effects of the atmospheric carbonation of
456 cementitious materials using reactive transport modelling, *Cem. Concr. Res.* 130 (2020) 105966.
457 doi:10.1016/j.cemconres.2019.105966.
- 458 [2] K. Ioannidou, K.J. Krakowiak, M. Bauchy, C.G. Hoover, E. Masoero, S. Yip, F.-J. Ulm, P. Levitz, R.J.-M.
459 Pellenq, E. Del Gado, Mesoscale texture of cement hydrates, *Proc. Natl. Acad. Sci.* 113 (2016) 2029–
460 2034. doi:10.1073/pnas.1520487113.
- 461 [3] J. Ollivier, J. Torrenti, La structure poreuse des bétons et les propriétés de transfert, *La Durabilité*
462 *Des Bétons.* (2008) 51–133.
- 463 [4] K.L. Scrivener, A.K. Crumbie, P. Laugesen, The Interfacial Transition Zone (ITZ) Between Cement
464 Paste and Aggregate in Concrete, *Interface Sci.* 12 (2004) 411–421.
465 doi:10.1023/B:INTS.0000042339.92990.4c.
- 466 [5] J.S. Dolado, K. van Breugel, Recent advances in modeling for cementitious materials, *Cem. Concr.*
467 *Res.* 41 (2011) 711–726. doi:10.1016/j.cemconres.2011.03.014.
- 468 [6] A. Dauzères, P. Le Bescop, P. Sardini, C. Cau Dit Coumes, Physico-chemical investigation of
469 clayey/cement-based materials interaction in the context of geological waste disposal:
470 Experimental approach and results, *Cem. Concr. Res.* 40 (2010) 1327–1340.
471 doi:10.1016/j.cemconres.2010.03.015.

- 472 [7] P. Lalan, A. Dauzères, L. De Windt, J. Sammaljärvi, D. Bartier, I. Techer, V. Detilleux, M. Siitari-
473 Kauppi, Mineralogical and microstructural evolution of Portland cement paste/argillite interfaces
474 at 70 °C – Considerations for diffusion and porosity properties, *Cem. Concr. Res.* 115 (2019) 414–
475 425. doi:10.1016/j.cemconres.2018.09.018.
- 476 [8] C. Carde, R. François, J.-M. Torrenti, Leaching of both calcium hydroxide and C-S-H from cement
477 paste: Modeling the mechanical behavior, *Cem. Concr. Res.* 26 (1996) 1257–1268.
478 doi:10.1016/0008-8846(96)00095-6.
- 479 [9] C. Carde, R. François, Effect of the leaching of calcium hydroxide from cement paste on mechanical
480 and physical properties, *Cem. Concr. Res.* 27 (1997) 539–550.
- 481 [10] E. Drouet, S. Poyet, P. Le Bescop, J.-M. Torrenti, X. Bourbon, Carbonation of hardened cement
482 pastes: Influence of temperature, *Cem. Concr. Res.* (2019).
483 doi:10.1016/j.cemconres.2018.09.019.
- 484 [11] D. Planel, J. Sercombe, P. Le Bescop, F. Adenot, J.M. Torrenti, Long-term performance of cement
485 paste during combined calcium leaching-sulfate attack: Kinetics and size effect, *Cem. Concr. Res.* 36
486 (2006) 137–143. doi:10.1016/j.cemconres.2004.07.039.
- 487 [12] X. Cong, R.J. Kirkpatrick, ²⁹Si MAS NMR study of the structure of calcium silicate hydrate, *Adv.*
488 *Cem. Based Mater.* 3 (1996) 144–156. doi:10.1016/S1065-7355(96)90046-2.
- 489 [13] A. Nonat, X. Lecoq, The Structure, Stoichiometry and Properties of C-S-H Prepared by C3S
490 Hydration Under Controlled Condition, in: P. Colombet, A.-R. Grimmer, H. Zanni, P. Sozzani (Eds.),
491 *Nucl. Magn. Reson. Spectrosc. Cem. Mater.*, Springer, 1998: pp. 197–207. doi:10.1007/978-3-642-
492 80432-8_14.
- 493 [14] I.F. Sáez Del Bosque, M. Martín-Pastor, I. Sobrados, S. Martínez-Ramírez, M.T. Blanco-Varela,
494 Quantitative analysis of pure triclinic tricalcium silicate and C-S-H gels by ²⁹Si NMR longitudinal
495 relaxation time, *Constr. Build. Mater.* 107 (2016) 52–57. doi:10.1016/j.conbuildmat.2015.12.146.
- 496 [15] K.O. Kjellsen, H. Justnes, Revisiting the microstructure of hydrated tricalcium silicate—a
497 comparison to Portland cement, *Cem. Concr. Compos.* 26 (2004) 947–956.
498 doi:10.1016/j.cemconcomp.2004.02.030.
- 499 [16] A. Helmuth, H. Turk, Elastic Moduli of Hardened Portland Cement and Tricalcium Silicate Pastes :
500 Effect of Porosity, *Portl. Cem. Assoc R D Lab Bull.* 144 (1966) 135–144.
- 501 [17] J. Hagymassy, I. Odler, M. Yudenfreund, J. Skalny, S. Brunauer, Pore structure analysis by water
502 vapor adsorption. III. Analysis of hydrated calcium silicates and portland cements, *J. Colloid*
503 *Interface Sci.* 38 (1972) 20–34. doi:10.1016/0021-9797(72)90215-9.
- 504 [18] G. Geng, R. Taylor, S. Bae, D. Hernández-Cruz, D.A. Kilcoyne, A.-H. Emwas, P.J.M. Monteiro, Atomic
505 and nano-scale characterization of a 50-year-old hydrated C3S paste, *Cem. Concr. Res.* 77 (2015)
506 36–46. doi:10.1016/j.cemconres.2015.06.010.
- 507 [19] E. Pustovgar, R.P. Sangodkar, A.S. Andreev, M. Palacios, B.F. Chmelka, R.J. Flatt, J.-B. d’Espinose de
508 Lacaillerie, Understanding silicate hydration from quantitative analyses of hydrating tricalcium
509 silicates, *Nat. Commun.* 7 (2016) 10952. doi:10.1038/ncomms10952.
- 510 [20] M. Codina, C. Cau-dit-Coumes, P. Le Bescop, J. Verdier, J.P. Ollivier, Design and characterization of
511 low-heat and low-alkalinity cements, *Cem. Concr. Res.* 38 (2008) 437–448.
512 doi:10.1016/j.cemconres.2007.12.002.
- 513 [21] H. Sakamoto, K. Haga, H. Fujita, K. Ishizaki, H. Amano, M. Hironaga, S. Nagasaki, S. Tanaka, pH
514 Behavior of Hydrated Low-Alkalinity Cement, *J. Nucl. Fuel Cycle Environ.* 5 (1999) 37–42.
515 doi:10.3327/jnuce.5.37.
- 516 [22] B. Lothenbach, G. Le Saout, M. Ben Haha, R. Figi, E. Wieland, Hydration of a low-alkali CEM III/B–
517 SiO₂ cement (LAC), *Cem. Concr. Res.* 42 (2012) 410–423. doi:10.1016/j.cemconres.2011.11.008.
- 518 [23] M. Auroy, S. Poyet, P. Le Bescop, J.M. Torrenti, T. Charpentier, M. Moskura, X. Bourbon, Impact of
519 carbonation on unsaturated water transport properties of cement-based materials, *Cem. Concr.*

- 520 Res. 74 (2015) 44–58. doi:10.1016/j.cemconres.2015.04.002.
- 521 [24] K. Iriya, A. Matsui, M. Mihara, Study on applicability of HFSC for radioactive waste repositories, in:
522 ASME (Ed.), *Radioact. Waste Manag. Environ. Remediat.* (ASME 1999), Nagoya (Japan), 1999.
523 doi:10.1081/E-EEE2-120046011.
- 524 [25] C. Cau Dit Coumes, S. Courtois, D. Nectoux, S. Leclercq, X. Bourbon, Formulating a low-alkalinity,
525 high-resistance and low-heat concrete for radioactive waste repositories, *Cem. Concr. Res.* 36
526 (2006) 2152–2163. doi:10.1016/j.cemconres.2006.10.005.
- 527 [26] J.J. Thomas, J.J. Chen, A.J. Allen, H.M. Jennings, Effects of decalcification on the microstructure and
528 surface area of cement and tricalcium silicate pastes, *Cem. Concr. Res.* 34 (2004) 2297–2307.
529 doi:10.1016/j.cemconres.2004.04.007.
- 530 [27] J.J. Chen, J.J. Thomas, H.M. Jennings, Decalcification shrinkage of cement paste, *Cem. Concr. Res.* 36
531 (2006) 801–809. doi:10.1016/j.cemconres.2005.11.003.
- 532 [28] J.J. Beaudoin, B. Patarachao, L. Raki, J. Margeson, R. Alizadeh, Length change of C–S–H of variable
533 composition immersed in aqueous solutions, *Adv. Cem. Res.* 22 (2010) 15–20.
534 doi:10.1680/adcr.2008.22.1.15.
- 535 [29] R.F. Feldman, Factors affecting young's modulus — Porosity relation of hydrated portland cement
536 compacts, *Cem. Concr. Res.* 2 (1972) 375–386. doi:10.1016/0008-8846(72)90054-3.
- 537 [30] P.J. Sereda, R.F. Feldman, Compacts of powdered material as porous bodies for use in sorption
538 studies, *J. Appl. Chem.* 13 (1963) 150–158. doi:10.1002/jctb.5010130402.
- 539 [31] Y. Wang, Q. Yuan, D. Deng, T. Ye, L. Fang, Measuring the pore structure of cement asphalt mortar by
540 nuclear magnetic resonance, *Constr. Build. Mater.* 137 (2017) 450–458.
541 doi:10.1016/j.conbuildmat.2017.01.109.
- 542 [32] W.A. Gutteridge, L.J. Parrott, A study of the changes in weight, length and interplanar spacing
543 induced by drying and rewetting synthetic CSH (I), *Cem. Concr. Res.* 6 (1976) 357–366.
544 doi:10.1016/0008-8846(76)90098-3.
- 545 [33] E.M. Foley, J.J. Kim, M.M.R. Taha, Synthesis and nano-mechanical characterization of calcium-
546 silicate-hydrate (C-S-H) made with 1.5 CaO / SiO₂ mixture, *Cem. Concr. Res.* 42 (2012) 1225–1232.
547 doi:10.1016/j.cemconres.2012.05.014.
- 548 [34] P. Pourbeik, J.J. Beaudoin, R. Alizadeh, L. Raki, Correlation between dynamic mechanical thermo-
549 analysis and composition-based models for C-S-H in hydrated portland cement paste, *Mater.*
550 *Struct.* 48 (2015) 2447–2454. doi:10.1617/s11527-014-0330-7.
- 551 [35] R. Khoshnazar, J.J. Beaudoin, L. Raki, R. Alizadeh, Durability and mechanical properties of C–S–
552 H/nitrobenzoic acid composite systems, *Mater. Struct.* 49 (2016) 5315–5325.
553 doi:10.1617/s11527-016-0862-0.
- 554 [36] E. Bernard, B. Lothenbach, C. Cau-Dit-Coumes, C. Chlique, A. Dauzères, I. Pochard, Magnesium and
555 calcium silicate hydrates, Part I: Investigation of the possible magnesium incorporation in calcium
556 silicate hydrate (C-S-H) and of the calcium in magnesium silicate hydrate (M-S-H), *Appl.*
557 *Geochemistry.* 89 (2018) 229–242. doi:10.1016/j.apgeochem.2017.12.005.
- 558 [37] E. Bernard, B. Lothenbach, F. Le Goff, I. Pochard, A. Dauzères, Effect of magnesium on calcium
559 silicate hydrate (C-S-H), *Cem. Concr. Res.* 97 (2017) 61–72. doi:10.1016/j.cemconres.2017.03.012.
- 560 [38] H. Yang, Y. Che, F. Leng, Calcium leaching behavior of cementitious materials in hydrochloric acid
561 solution, *Sci. Rep.* 8 (2018) 1–9. doi:10.1038/s41598-018-27255-x.
- 562 [39] Y.S. Choi, E.I. Yang, Effect of calcium leaching on the pore structure, strength, and chloride
563 penetration resistance in concrete specimens, *Nucl. Eng. Des.* 259 (2013) 126–136.
564 doi:10.1016/j.nucengdes.2013.02.049.
- 565 [40] P.J. Sereda, R.F. Feldman, E.G. Swenson, Effect of sorbed water on some mechanical properties of
566 hydrated Portland cement pastes and compacts, *Spec. Rep. Highw. Res. Board.* 90 (1967) 58–73.
567 doi:10.1039/J19710002393.

- 568 [41] W. Kunther, S. Ferreiro, J. Skibsted, Influence of the Ca/Si ratio on the compressive strength of
569 cementitious calcium-silicate-hydrate binders, *J. Mater. Chem. A* 5 (2017) 17401–17412.
570 doi:10.1039/c7ta06104h.
- 571 [42] R. Maddalena, K. Li, P.A. Chater, S. Michalik, A. Hamilton, Direct synthesis of a solid calcium-silicate-
572 hydrate (C-S-H), *Constr. Build. Mater.* 223 (2019) 554–565.
573 doi:10.1016/j.conbuildmat.2019.06.024.
- 574 [43] L.G. Li, J.Y. Zheng, J. Zhu, A.K.H. Kwan, Combined usage of micro-silica and nano-silica in concrete:
575 SP demand, cementing efficiencies and synergistic effect, *Constr. Build. Mater.* 168 (2018) 622–
576 632. doi:10.1016/j.conbuildmat.2018.02.181.
- 577 [44] L. Nicoleau, A. Nonat, D. Perrey, The di- and tricalcium silicate dissolutions, *Cem. Concr. Res.* 47
578 (2013) 14–30. doi:10.1016/j.cemconres.2013.01.017.
- 579 [45] S. Garrault, Study of C-S-H growth on C3S surface during its early hydration, *Mater. Struct.* 38
580 (2005) 435–442. doi:10.1617/14343.
- 581 [46] H.F.W. Taylor, *Cement chemistry*, 2nd ed., Academic Press, London (UK), 1990.
582 doi:10.1016/S0958-9465(98)00023-7.
- 583 [47] C. Rößler, F. Steiniger, H.-M. Ludwig, Characterization of C-S-H and C-A-S-H phases by electron
584 microscopy imaging, diffraction, and energy dispersive X-ray spectroscopy, *J. Am. Ceram. Soc.* 100
585 (2017) 1733–1742. doi:10.1111/jace.14729.
- 586 [48] Z.-Q. Wu, J.F. Young, The hydration of tricalcium silicate in the presence of colloidal silica, *J. Mater.*
587 *Sci.* 19 (1984) 3477–3486. doi:10.1007/BF02396922.
- 588 [49] K.O. Kjellsen, B. Lagerblad, Microstructure of tricalcium silicate and Portland cement systems at
589 middle periods of hydration-development of Hadley grains, *Cem. Concr. Res.* 37 (2007) 13–20.
590 doi:10.1016/j.cemconres.2006.09.008.
- 591 [50] M. Atkins, E.E. Lachowski, F.P. Glasser, Investigation of solid and aqueous chemistry of 10-year-old
592 Portland cements pastes; with and without silica modifier, *Adv. Cem. Res.* 5 (1993) 97–102.
- 593 [51] K. Baltakys, R. Jauberthie, R. Jauberthie, R. Siauciunas, R. Kaminskas, Influence of modification of
594 SiO₂ on the formation of calcium silicate hydrate, *Mater. Sci.* 25 (2007) 663–670.
- 595 [52] R. Maddalena, C. Hall, A. Hamilton, Effect of silica particle size on the formation of calcium silicate
596 hydrate [C-S-H] using thermal analysis, *Thermochim. Acta.* 672 (2019) 142–149.
597 doi:10.1016/j.tca.2018.09.003.
- 598 [53] Z. Rong, W. Sun, H. Xiao, G. Jiang, Effects of nano-SiO₂ particles on the mechanical and
599 microstructural properties of ultra-high performance cementitious composites, *Cem. Concr.*
600 *Compos.* 56 (2015) 25–31. doi:10.1016/j.cemconcomp.2014.11.001.
- 601 [54] G. Quercia, G. Hüsken, H.J.H. Brouwers, Water demand of amorphous nano silica and its impact on
602 the workability of cement paste, *Cem. Concr. Res.* 42 (2012) 344–357.
603 doi:10.1016/j.cemconres.2011.10.008.
- 604 [55] S. Abd.El.Aleem, M. Heikal, W.M. Morsi, Hydration characteristic, thermal expansion and
605 microstructure of cement containing nano-silica, *Constr. Build. Mater.* 59 (2014) 151–160.
606 doi:10.1016/j.conbuildmat.2014.02.039.
- 607 [56] R.K. Iler, Coagulation of colloidal silica by calcium ions, mechanism, and effect of particle size, *J.*
608 *Colloid Interface Sci.* 53 (1975) 476–488. doi:10.1016/0021-9797(75)90065-X.
- 609 [57] E.A. Gorrepati, P. Wongthahan, S. Raha, H.S. Fogler, Silica precipitation in acidic solutions:
610 Mechanism, pH effect, and salt effect, *Langmuir.* 26 (2010) 10467–10474. doi:10.1021/la904685x.
- 611 [58] V. Dutzer, W. Dridi, S. Poyet, P. Le Bescop, X. Bourbon, The link between gas diffusion and
612 carbonation in hardened cement pastes, *Cem. Concr. Res.* 123 (2019) 105795.
613 doi:10.1016/j.cemconres.2019.105795.
- 614 [59] T.L.P. Hang, J. Verdier, T. Vidal, G. Camps, X. Bourbon, Mechanical and transfer properties of low-pH

- 615 concretes in view of classical HPC substitution in confinement structures, *Eur. J. Environ. Civ. Eng.*
616 23 (2019) 657–674. doi:10.1080/19648189.2017.1304274.
- 617 [60] M.C. Alonso, J.L. García Calvo, S. Petterson, I. Puigdomenech, M.A. Cunado, M. Vuorio, H. Weber, H.
618 Ueda, M. Naito, C. Walker, Y. Takeshi, C. Cau Dit Coumes, Round Robin test for define an accurate
619 protocol to measure the pore fluid pH of low-pH cementitious materials, in: SFEN (Ed.), *Proc. 2nd*
620 *Int. Symp. Cem. Mater. Nucl. Wastes*, SFEN, Avignon, France, 2014: pp. 1–10.
- 621 [61] A. Behnood, K. van Tittelboom, N. de Belie, Methods for measuring pH in concrete : A review,
622 *Constr. Build. Mater.* 105 (2016) 176–188. doi:10.1016/j.conbuildmat.2015.12.032.
- 623 [62] G. Plusquellec, M.R. Geiker, J. Lindgård, J. Duchesne, B. Fournier, K. De Weerd, Determination of
624 the pH and the free alkali metal content in the pore solution of concrete: Review and experimental
625 comparison, *Cem. Concr. Res.* 96 (2017) 13–26. doi:10.1016/j.cemconres.2017.03.002.
- 626 [63] G. Villain, M. Thiery, G. Platret, Measurement methods of carbonation profiles in concrete:
627 thermogravimetry, chemical analysis and gammadensimetry, *Cem. Concr. Res.* 37 (2007) 1182–
628 1192. doi:10.1016/j.cemconres.2007.04.015.
- 629 [64] B. Lothenbach, P. Durdzinski, K. De Weerd, Thermogravimetric analysis, in: K. Scrivener, R.
630 Snellings, B. Lothenbach (Eds.), *A Pract. Guid. to Microstruct. Anal. Cem. Mater.*, CRC Press, Boca
631 Raton (USA), 2016: pp. 177–211.
- 632 [65] F. Angeli, M. Gaillard, P. Jollivet, T. Charpentier, Contribution of ^{43}Ca MAS NMR for probing the
633 structural configuration of calcium in glass, *Chem. Phys. Lett.* 440 (2007) 324–328.
634 doi:10.1016/j.cplett.2007.04.036.
- 635 [66] T. Charpentier, Résonance magnétique nucléaire haute-résolution des noyaux quadrupolaires dans
636 les solides. PhD thesis, (in French), 1998.
- 637 [67] AFNOR, Essai pour béton durci : essai de porosité et de masse volumique (in French), *Stand. NF*
638 *P18-459*. (2010) 9p.
- 639 [68] R.A. Olson, H.M. Jennings, Estimation of C-S-H content in a blended cement paste using water
640 adsorption, *Cem. Concr. Res.* 31 (2001) 351–356. doi:10.1016/S0008-8846(01)00454-9.
- 641 [69] S. Poyet, K. Trentin, E. Amblard, The Use of Sorption Balance for the Characterization of the Water
642 Retention Curve of Cement-Based Materials, *J. Adv. Concr. Technol.* 14 (2016) 354–367.
643 doi:10.3151/jact.14.354.
- 644 [70] G.W. Groves, A. Brough, I.G. Richardson, C.M. Dobson, Progressive changes in the structure of
645 hardened C3S cement pastes due to carbonation, *J. Am. Ceram. Soc.* 74 (1991) 2891–2896.
- 646 [71] I.G. Richardson, G.W. Groves, Models for the composition and structure of calcium silicate hydrate
647 (CSH) gel in hardened tricalcium silicate pastes, *Cem. Concr. Res.* 22 (1992) 1001–1010.
648 doi:10.1016/0008-8846(92)90030-Y.
- 649 [72] J.W. Bullard, J. Hagedorn, T.M. Ley, Q. Hu, W. Griffin, J.E. Terrill, A critical comparison of 3D
650 experiments and simulations of tricalcium silicate hydration, *J. Am. Ceram. Soc.* 101 (2018) 1453–
651 1470. doi:10.1111/jace.15323.
- 652 [73] Z. Xu, Z. Zhou, P. Du, X. Cheng, Effects of nano-silica on hydration properties of tricalcium silicate,
653 *Constr. Build. Mater. J.* 125 (2016) 1169–1177. doi:10.1016/j.conbuildmat.2016.09.003.
- 654 [74] S. Grangeon, F. Claret, Y. Linard, C. Chiaberge, X-ray diffraction: A powerful tool to probe and
655 understand the structure of nanocrystalline calcium silicate hydrates, *Acta Crystallogr. Sect. B*
656 *Struct. Sci. Cryst. Eng. Mater.* 69 (2013) 465–473. doi:10.1107/S2052519213021155.
- 657 [75] S. Merlino, E. Bonaccorsi, T. Armbruster, The real structure of tobermorite 11A: normal and
658 anomalous forms, OD character and polytypic modifications, *Eur. J. Mineral.* 13 (2001) 577–590.
659 doi:10.1127/0935-1221/2001/0013-0577.
- 660 [76] E. Bonaccorsi, S. Merlino, H.F.W. Taylor, The crystal structure of jennite, $\text{Ca}_9\text{Si}_6\text{O}_{18}(\text{OH})_6 \cdot 8\text{H}_2\text{O}$,
661 *Cem. Concr. Res.* 34 (2004) 1481–1488. doi:10.1016/j.cemconres.2003.12.033.

- 662 [77] A. Dauzères, Etude expérimentale et modélisation des mécanismes physico-chimiques des
663 interactions béton-argile dans le contexte du stockage géologique des déchets radioactifs (in
664 french), Ph.D. Thesis, University Poitiers (France), 2010.
- 665 [78] M. Auroy, Impact de la carbonatation sur les propriétés de transport d'eau des matériaux
666 cimentaires (in french), Ph.D. Thesis, Université Paris-Est (France), 2014.
- 667 [79] E. Drouet, S. Poyet, J.-M. Torrenti, Temperature influence on water transport in hardened cement
668 pastes, *Cem. Concr. Res.* 76 (2015) 37–50. doi:10.1016/j.cemconres.2015.05.002.
- 669 [80] I. Klur, B. Pollet, J. Virlet, A. Nonat, C-S-H Structure Evolution with Calcium Content by Multinuclear
670 NMR, in: *Nucl. Magn. Reson. Spectrosc. Cem. Mater.*, Springer Berlin Heidelberg, Berlin, Heidelberg,
671 1998: pp. 119–141. doi:10.1007/978-3-642-80432-8_8.
- 672 [81] M.D. Andersen, H.J. Jakobsen, J. Skibsted, Characterization of white Portland cement hydration and
673 the C-S-H structure in the presence of sodium aluminate by ²⁷Al and ²⁹Si MAS NMR spectroscopy,
674 *Cem. Concr. Res.* 34 (2004) 857–868. doi:10.1016/j.cemconres.2003.10.009.
- 675 [82] I. Klur, J.-F. Jacquinet, F. Brunet, T. Charpentier, J. Virlet, C. Schneider, P. Tekely, NMR Cross-
676 Polarization when $T_{IS} > T_{1\rho}$; Examples from Silica Gel and Calcium Silicate Hydrates, *J. Phys.*
677 *Chem. B.* 104 (2000) 10162–10167. doi:10.1021/jp001342u.
- 678 [83] T.F. Sevelsted, J. Skibsted, Carbonation of C-S-H and C-A-S-H samples studied by ¹³C, ²⁷Al and ²⁹Si
679 MAS NMR spectroscopy, *Cem. Concr. Res.* 71 (2015) 56–65. doi:10.1016/j.cemconres.2015.01.019.
- 680 [84] S. Grangeon, F. Claret, C. Roosz, T. Sato, S. Gaboreau, Y. Linard, Structure of nanocrystalline calcium
681 silicate hydrates: Insights from X-ray diffraction, synchrotron X-ray absorption and nuclear
682 magnetic resonance, *J. Appl. Crystallogr.* 49 (2016) 771–783. doi:10.1107/S1600576716003885.
- 683 [85] I.G. Richardson, G.W. Groves, Microstructure and microanalysis of hardened ordinary Portland
684 cement pastes, *J. Mater. Sci.* 28 (1993) 265–277. doi:10.1007/BF00349061.
- 685 [86] J.E. Rossen, B. Lothenbach, K.L. Scrivener, Composition of C-S-H in pastes with increasing levels of
686 silica fume addition, *Cem. Concr. Res.* 75 (2015) 14–22. doi:10.1016/j.cemconres.2015.04.016.
- 687 [87] J. Haas, A. Nonat, From C-S-H to C-A-S-H: Experimental study and thermodynamic modelling, *Cem.*
688 *Concr. Res.* 68 (2015) 124–138. doi:10.1016/j.cemconres.2014.10.020.
- 689 [88] E.P. Flint, L.S. Wells, Study of the system CaO-SiO₂-H₂O at 30 C and of the reaction of water on the
690 anhydrous calcium silicates, *Bur. Stand. J. Res.* 12 (1934) 33. doi:10.6028/jres.012.060.
- 691 [89] M. Grutzeck, A. Benesi, B. Fanning, Silicon-29 Magic Angle Spinning Nuclear Magnetic Resonance
692 Study of Calcium Silicate Hydrates, *J. Am. Ceram. Soc.* 72 (1989) 665–668.
693 <http://onlinelibrary.wiley.com/doi/10.1111/j.1151-2916.1989.tb06192.x/abstract>.
- 694 [90] J.J. Chen, J.J. Thomas, H.F.W. Taylor, H.M. Jennings, Solubility and structure of calcium silicate
695 hydrate, *Cem. Concr. Res.* 34 (2004) 1499–1519. doi:10.1016/j.cemconres.2004.04.034.
- 696 [91] S.A. Greenberg, T.N. Chang, Investigation of the Colloidal Hydrated Calcium Silicates. II. Solubility
697 Relationships in the Calcium Oxide-Silica-Water System at 25°, *J. Phys. Chem.* 69 (1965) 182–188.
698 doi:10.1021/j100885a027.
- 699 [92] K. Suzuki, T. Nishikawa, S. Ito, Formation and carbonation of C-S-H in water, *Cem. Concr. Res.* 15
700 (1985) 213–224. doi:10.1016/0008-8846(85)90032-8.
- 701 [93] A. Atkinson, J.A. Hearne, C.F. Knights, Aqueous chemistry and thermodynamic modelling of CaO-
702 SiO₂-H₂O gels, *J. Chem. Soc., Dalt. Trans.* 0 (1989) 2371–2379. doi:10.1039/DT9890002371.
- 703 [94] M. Atkins, F.P. Glasser, A. Kindness, Cement hydrate phase: Solubility at 25°C, *Cem. Concr. Res.* 22
704 (1992) 241–246. doi:10.1016/0008-8846(92)90062-Z.
- 705 [95] A. Harris, M. Manning, W. Tearle, C. Tweed, Testing of models of the dissolution of cements—
706 leaching of synthetic CSH gels, *Cem. Concr. Res.* 32 (2002) 731–746. doi:10.1016/S0008-
707 8846(01)00748-7.

- 708 [96] J. Hill, A.W. Harris, M. Manning, A. Chambers, S.W. Swanton, The effect of sodium chloride on the
709 dissolution of calcium silicate hydrate gels, *Waste Manag.* 26 (2006) 758–768.
710 doi:<https://doi.org/10.1016/j.wasman.2006.01.022>.
- 711 [97] C.S. Walker, D. Savage, M. Tyrer, K.V. Ragnarsdottir, Non-ideal solid solution aqueous solution
712 modeling of synthetic calcium silicate hydrate, *Cem. Concr. Res.* 37 (2007) 502–511.
713 doi:[10.1016/j.cemconres.2006.12.002](https://doi.org/10.1016/j.cemconres.2006.12.002).
- 714 [98] D. Sugiyama, Chemical alteration of calcium silicate hydrate (C–S–H) in sodium chloride solution,
715 *Cem. Concr. Res.* 38 (2008) 1270–1275. doi:[10.1016/j.cemconres.2008.06.002](https://doi.org/10.1016/j.cemconres.2008.06.002).
- 716 [99] V.S. Ramachandran, Interaction of calcium lignosulfonate with tricalcium silicate, hydrated
717 tricalcium silicate and calcium hydroxide, *Cem. Concr. Resear.* 2 (1972) 179–194.
- 718 [100] R. Flatt, I. Schober, Superplasticizers and the rheology of concrete, in: N. Roussel (Ed.), *Underst.*
719 *Rheol. Concr.*, Woodhead Publishing Limited, 2012: pp. 144–208.
720 doi:[10.1533/9780857095282.2.144](https://doi.org/10.1533/9780857095282.2.144).
- 721 [101] A. Popova, G. Geoffroy, M.-F. Renou-Gonnord, P. Faucon, E. Gartner, Interactions between
722 Polymeric Dispersants and Calcium Silicate Hydrates, *J. Am. Ceram. Soc.* 83 (2000) 2556–2560.
723 doi:[10.1111/j.1151-2916.2000.tb01590.x](https://doi.org/10.1111/j.1151-2916.2000.tb01590.x).
- 724 [102] A. Popova, G. Geoffroy, E.M. Gartner, A. Lapp, Calcium Silicate Hydrates studied by Small-Angle
725 Neutron Scattering (SANS), *J. Am. Ceram. Soc.* 85 (2002) 1303–1305.
- 726 [103] J. Sun, H. Shi, B. Qian, Z. Xu, W. Li, X. Shen, Effects of synthetic C-S-H/PCE nanocomposites on early
727 cement hydration, *Constr. Build. Mater.* 140 (2017) 282–292.
728 doi:[10.1016/j.conbuildmat.2017.02.075](https://doi.org/10.1016/j.conbuildmat.2017.02.075).
- 729 [104] V. Kanchanason, J. Plank, Role of pH on the structure, composition and morphology of C-S-H–PCE
730 nanocomposites and their effect on early strength development of Portland cement, *Cem. Concr.*
731 *Res.* 102 (2017) 90–98. doi:[10.1016/j.cemconres.2017.09.002](https://doi.org/10.1016/j.cemconres.2017.09.002).
- 732 [105] J. Plank, M. Schönlein, V. Kanchanason, Study on the early crystallization of calcium silicate hydrate
733 (C-S-H) in the presence of polycarboxylate superplasticizers, *J. Organomet. Chem.* 869 (2018) 227–
734 232. doi:[10.1016/j.jorganchem.2018.02.005](https://doi.org/10.1016/j.jorganchem.2018.02.005).
- 735 [106] V. Kanchanason, J. Plank, Effectiveness of a calcium silicate hydrate – Polycarboxylate ether (C-S-
736 H–PCE) nanocomposite on early strength development of fly ash cement, *Constr. Build. Mater.* 169
737 (2018) 20–27. doi:[10.1016/j.conbuildmat.2018.01.053](https://doi.org/10.1016/j.conbuildmat.2018.01.053).
- 738 [107] I.G. Richardson, Model structures for C-(A)-S-H(I), *Acta Crystallogr. Sect. B Struct. Sci. Cryst. Eng.*
739 *Mater.* 70 (2014) 903–923. doi:[10.1107/S2052520614021982](https://doi.org/10.1107/S2052520614021982).
- 740 [108] A. Nonat, The structure and stoichiometry of C-S-H, *Cem. Concr. Res.* 34 (2004) 1521–1528.
741 doi:[10.1016/j.cemconres.2004.04.035](https://doi.org/10.1016/j.cemconres.2004.04.035).
- 742 [109] I. García-Lodeiro, A. Fernández-Jiménez, I. Sobrados, J. Sanz, A. Palomo, C-S-H gels: Interpretation
743 of ²⁹Si MAS-NMR spectra, *J. Am. Ceram. Soc.* 95 (2012) 1440–1446. doi:[10.1111/j.1151-2916.2012.05091.x](https://doi.org/10.1111/j.1151-2916.2012.05091.x).
- 744
- 745 [110] Y. He, L. Lu, L.J. Struble, J.L. Rapp, P. Mondal, S. Hu, Effect of calcium–silicon ratio on microstructure
746 and nanostructure of calcium silicate hydrate synthesized by reaction of fumed silica and calcium
747 oxide at room temperature, *Mater. Struct.* 47 (2013) 311–322. doi:[10.1617/s11527-013-0062-0](https://doi.org/10.1617/s11527-013-0062-0).
- 748 [111] E. L’Hôpital, B. Lothenbach, D.A. Kulik, K. Scrivener, Influence of calcium to silica ratio on
749 aluminium uptake in calcium silicate hydrate, *Cem. Concr. Res.* 85 (2016) 111–121.
750 doi:[10.1016/j.cemconres.2016.01.014](https://doi.org/10.1016/j.cemconres.2016.01.014).
- 751 [112] R.J. Myers, S.A. Bernal, R. San Nicolas, J.L. Provis, Generalized structural description of calcium-
752 sodium aluminosilicate hydrate gels: The cross-linked substituted tobermorite model, *Langmuir.*
753 29 (2013) 5294–5306. doi:[10.1021/la4000473](https://doi.org/10.1021/la4000473).

755 **Supplementary materials**

756

757 **Appendix A: details of the batching sequence.**

758 The final batching sequence obtained for the model pastes including nanosilica was as follows:

- 759 1. Addition of C₃S in the planetary mixer (mixing speed at 95 rpm).
760 2. Addition of all the water, including half of the total amount of SP.
761 3. Mixing at 250 rpm for 30 s.
762 4. Slow incorporation of nanosilica (at 400 rpm) while monitoring the fresh mix rheology
763 to avoid flocculation and a viscosity increase that could eventually make it irreversibly
764 unworkable. Addition of SP to maintain the workability of the fresh mix. The duration of
765 this step depended on the amount of nanosilica added (Table 1).
766 5. Preparation of the test specimens: the paste was poured into polytetrafluoroethylene
767 (PTFE) moulds (Ø30 × H110 mm) and vibrated. This phase proved complicated due to
768 the strong thixotropic behaviour of the fresh mix, which worsened when the silica
769 content was increased.
770 6. The specimens were kept one month in their sealed moulds at ambient temperature.
771 After unmoulding, they were cured for two more months under a batch of water to
772 which small amounts of crushed samples were added to ensure that chemical
773 equilibrium was reached in the curing solution.
774 7. Finally, the samples were left to dry in a glovebox at 20°C and 55% RH. It is presumed
775 that under these conditions, hydration did not proceed significantly anymore.

776

777

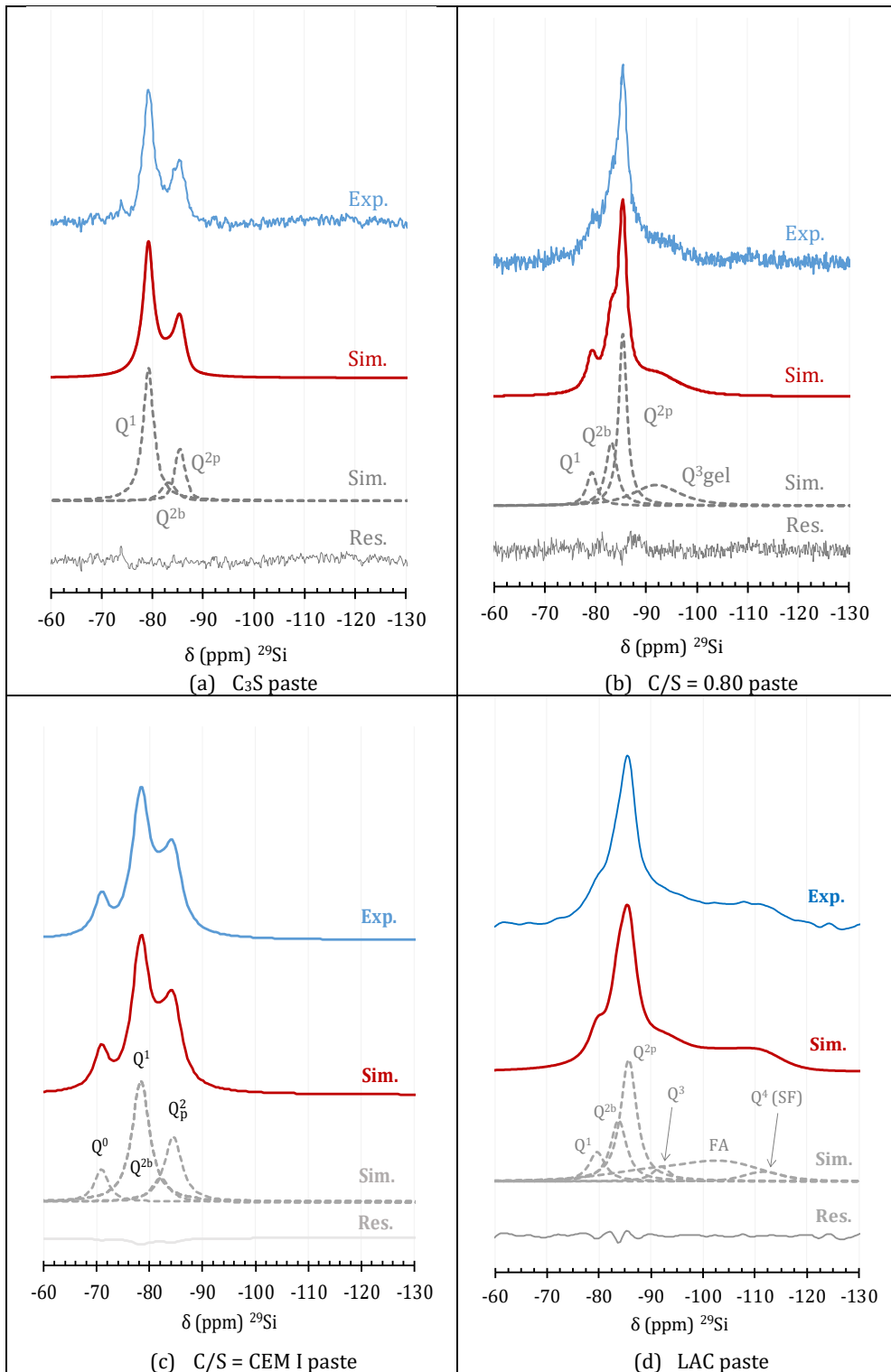


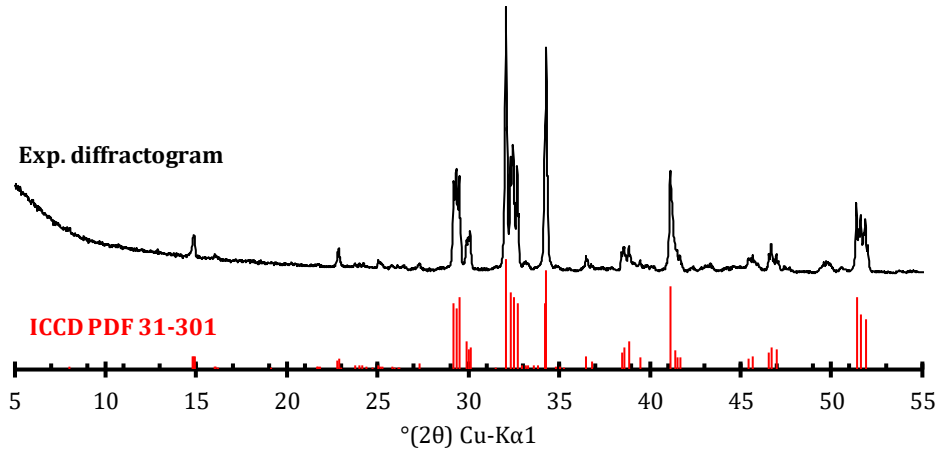
Figure S 1: Examples of decomposition of ^{29}Si NMR spectra.

Table S 1: Parameters of the decomposition of the ^{29}Si NMR spectra of the synthetic pastes. No Q^0 peak was considered for the C_3S paste as its contribution was of the order of the noise.

C/S ratio		0.8-3.00
Q ¹	δ (ppm)	-79.2
	FWHM (ppm)	2.9
	Ratio L/G	1.0
	GB	1.02
Q ^{2_b}	δ (ppm)	-83.1
	FWHM (ppm)	2.9
	Ratio L/G	0.5
	GB	1.1
Q ^{2_p}	δ (ppm)	-85.4
	FWHM (ppm)	2.21
	Ratio L/G	1.0
	GB	0.5
Q ³ + Q ^{3gel}	δ (ppm)	-92
	FWHM (ppm)	11.3
	Ratio L/G	0.5
	GB (ppm)	4.7
G = Gaussian lineshape L = Lorentzian lineshape GB = Gaussian enhancement		

794 **Appendix D: Chemical composition of the components of the synthetic model and**
 795 **reference pastes**

796



797

798 *Figure S 3: diffractogram of the C₃S used for the preparation of the synthetic model pastes*

799

800 **Main properties of the colloidal silica suspension (Rheomac AS 150):**

- 801 • density = 1.40 ± 0.02 g.cm⁻³;
- 802 • pH = 10 ± 1.5;
- 803 • Cl < 0.1 wt%;
- 804 • Na₂O_{eq} < 1.0 wt%

805

806 *Table S 2: chemical composition of the LAC reference pastes' components, reproduced from [20]*

Compounds	wt% of the compounds			wt% of the blend (LAC)
	CEM I 52.5	Silica fume	Fly Ash	
	Lafarge Le Teil	Condensil S95 DM	EDF Cordemais	
CaO	67.41	0.40	5.52	27.0
SiO ₂	22.84	95.00	49.48	54.3
Al ₂ O ₃	2.70	0.60	29.17	10.0
Fe ₂ O ₃	1.84	<0.05	6.23	2.6
MgO	0.81	0.30	2.08	1.0
MnO	-	-	0.08	-
Na ₂ O	0.14	<0.20	0.58	0.3
K ₂ O	0.23	0.29	1.22	0.5
SO ₃	2.23	<0.20	0.64	1.1
S ²⁻	<0.01	<0.10	-	
P ₂ O ₅	-	-	0.70	
TiO ₂	-	-	1.61	
LOI	1.72	3.10	2.20	

LOI = loss on ignition (1000 °C)

807

808

809

810 *Table S 3: chemical composition of the OPC used for the preparation of the OPC reference paste*

Compounds	CEM I 52.5
	Lafarge Val d'Azergues
CaO	65.0
SiO ₂	21.0
Al ₂ O ₃	3.4
Fe ₂ O ₃	4.5
MgO	0.62
MnO	-
Na ₂ O	0.09
K ₂ O	0.72
SO ₃	2.71
S ²⁻	<0.01
P ₂ O ₅	0.50
TiO ₂	-
LOI	1.30
LOI = Loss on ignition (1000 °C)	